

A void in the Hubble tension? The end of the line for the Hubble bubble

David Camarena,¹ Valerio Marra,^{2,3,4} Ziad Sakr,⁵ and Chris Clarkson^{6,7,8}

¹PPGCosmo, Universidade Federal do Espírito Santo, 29075-910, Vitória, ES, Brazil

²Núcleo de Astrofísica e Cosmologia & Departamento de Física, Universidade Federal do Espírito Santo, 29075-910, Vitória, ES, Brazil

³INAF – Osservatorio Astronomico di Trieste, via Tiepolo 11, 34131, Trieste, Italy

⁴IFPU – Institute for Fundamental Physics of the Universe, via Beirut 2, 34151, Trieste, Italy

⁵Université St Joseph; Faculty of Sciences, Beirut, Lebanon

⁶Department of Physics and Astronomy, Queen Mary University of London, UK

⁷Department of Physics & Astronomy, University of the Western Cape, Cape Town 7535, South Africa

⁸Department of Mathematics & Applied Mathematics, University of Cape Town, Cape Town 7701, South Africa

August 9, 2022

ABSTRACT

The Universe may feature large-scale inhomogeneities beyond the standard paradigm, implying that statistical homogeneity and isotropy may be reached only on much larger scales than the usually assumed ~ 100 Mpc. This means that we are not necessarily typical observers and that the Copernican principle could be recovered only on super-Hubble scales. Here, we do not assume the validity of the Copernican principle and let Cosmic Microwave Background, Baryon Acoustic Oscillations, type Ia supernovae, local H_0 , cosmic chronometers, Compton γ -distortion and kinetic Sunyaev–Zeldovich observations constrain the geometrical degrees of freedom of the local structure, which we parametrize via the ALTB model—basically a non-linear radial perturbation of a FLRW metric. In order to quantify if a non-Copernican structure could explain away the Hubble tension, we pay careful attention to computing the Hubble constant in an inhomogeneous universe, and we adopt model selection via both the Bayes factor and the Akaike information criterion. Our results show that, while the ALTB model can successfully explain away the H_0 tension, it is favored with respect to the Λ CDM model only if one solely considers supernovae in the redshift range that is used to fit the Hubble constant, that is, $0.023 < z < 0.15$. If one considers all the supernova sample, then the H_0 tension is not solved and the support for the ALTB model vanishes. Combined with other data sets, this solution to the Hubble tension barely helps. Finally, we have reconstructed our local spacetime. We have found that data are best fit by a shallow void with $\delta_L \approx -0.04$ and $r_L^{\text{out}} \approx 300$ Mpc, which, interestingly, lies on the border of the 95% credible region relative to the standard model expectation.

Key words: large-scale structure of Universe – cosmology: observations – cosmological parameters – cosmology: theory

1 INTRODUCTION

Accurate cosmological and astrophysical observations have revealed a discrepancy between early- and late-time determinations of the Hubble constant. This discrepancy, with a significance of 5σ if one considers CMB observations (Aghanim et al. 2018) and the local cosmic distance ladder (Riess et al. 2021), is the so-called Hubble tension. In the absence of unknown systematic errors, this discrepancy could suggest the existence of physics beyond the standard paradigm of cosmology. This scenario has led cosmologists to propose and study new cosmological models, mainly, but not limited to, those that extend the Λ CDM model at early- or late-times

(see Abdalla et al. 2022, for an up-to-date and extensive review).

Although many of the models proposed to solve the Hubble tension involve modifications to dark matter and dark energy or changes to the theory of gravity, geometrical degrees of freedom have also been considered. Indeed, within the standard model, the universe is expected to be homogeneous and isotropic only at scales $\gtrsim 100$ Mpc so that we may need to take into account the local perturbed spacetime when analyzing observations at low redshifts. This may be relevant for the Hubble tension as the H_0 measurement

of [Riess et al. \(2021\)](#) is based on the luminosity-distance-redshift relation in the redshift range $0.023 < z < 0.15$.

At the linear level, an adiabatic perturbation in the density of our local spacetime causes a perturbation in the expansion rate given by ([Marra et al. 2013](#)):

$$\frac{\delta H_0}{H_0} = -\frac{1}{3} f(\Omega_m) \frac{\delta \rho(t_0)}{\rho(t_0)}, \quad (1)$$

where $f \simeq 0.5$ is the present-day growth rate for the concordance Λ CDM model. One can then see how a local underdensity, $\delta\rho/\rho < 0$, would cause a higher local expansion rate, $\delta H_0/H_0 > 0$. However, perturbations are smaller on larger scales and the typical contrast – i.e., dictated by the amplitude of perturbations as constrained by CMB observations within the standard Λ CDM model – quickly decreases so that the homogeneous FLRW limit is reached. Theoretical computations (see [Camarena & Marra 2018](#), and references therein) and numerical simulations (see [Odderskov et al. 2017](#), and references therein) suggest that this cosmic variance on H_0 causes a 0.5–1% systematic uncertainty when analyzing observations in the redshift range $0.023 < z < 0.15$, falling short of explaining the 9% difference between early- and late-times constraints.

This failure in explaining away the Hubble tension is due to the fact that we assumed the standard spectrum of perturbations which is based on a series of assumptions, such as the Copernican principle, the use of the FLRW metric and standard slow-roll inflation. However, the Universe may feature large-scale inhomogeneities beyond the standard paradigm, that is, statistical homogeneity and isotropy may be reached only on much larger scales than the usually assumed 100 Mpc. In other words, we are not necessarily typical observers and the Copernican principle could be recovered only on grander scales so that observations could depend on the position of the observer and the notion of an average FLRW observer would cease to be meaningful ([Kolb et al. 2010](#)). This could tremendously modify our perception of the cosmos and motivates us to take a pragmatic approach and test if a local inhomogeneity of any size and depth could solve the H_0 tension.

There has been growing observational evidence that the local universe is underdense on scales of several hundred megaparsecs, as reported by [Frith et al. \(2003\)](#); [Keenan et al. \(2013\)](#); [Whitbourn & Shanks \(2014\)](#); [Hoscheit & Barger \(2018\)](#); [Haslbauer et al. \(2020\)](#); [Böhringer et al. \(2020\)](#); [Wong et al. \(2021\)](#). Furthermore, several anomalous signals in cosmological observables have been emerging since the establishment of the Λ CDM model as the standard model of cosmology more than two decades ago. Besides the Hubble crisis, particularly relevant here are the CMB anomalies and the cosmic dipoles (see [Perivolaropoulos & Skara 2021](#), and references therein). These signals are at odds with the standard paradigm according to which the spacetime is well described by the homogeneous and isotropic FLRW metric on scales larger than ≈ 100 Mpc.

In [Camarena et al. \(2022\)](#), we tested if the Copernican Principle is valid, that is, if we are indeed ‘typical’ FLRW observers. Specifically, we have probed radial inhomogeneity around us by constraining the ALTB model with the latest available data from CMB, BAO, type Ia supernovae, local H_0 , cosmic chronometers, Compton γ -distortion, and kinetic Sunyaev–Zeldovich effect. The ALTB model is basically the

Λ CDM model with the addition of an arbitrary spherical inhomogeneity. We found that inhomogeneity around us approximately follows the expectation of the standard model.

Here, we extend the results of [Camarena et al. \(2022\)](#) in order to reconstruct our local spacetime and test its implications for the Hubble tension. Special attention is given to the method used to measure the local Hubble constant in an inhomogeneous Universe, Bayesian model comparison, and a generalization of the LTB profile in order to better reconstruct our cosmological neighborhood.

Similar analyses using the ALTB model were carried out by [Tokutake et al. \(2018\)](#); [Hoscheit & Barger \(2018\)](#); [Kenworthy et al. \(2019\)](#); [Luković et al. \(2020\)](#); [Ding et al. \(2020\)](#); [Cai et al. \(2021\)](#); [Castello et al. \(2021\)](#). [Kenworthy et al. \(2019\)](#) looked at the luminosity distance-redshift relation of 1295 SNe over a redshift range of $0.01 < z < 2.26$ and concluded that data is inconsistent at the 4–5 σ confidence level with a large local underdensity with $\delta < -0.2$ so that local H_0 measurements are not affected by the local structure. [Luković et al. \(2020\)](#) confronted luminosity data from 35000 galaxies in the range $0.005 < z < 0.2$ with the ALTB model, finding support for a deep void ([Keenan et al. 2013](#)). However, the comparison with supernova data did not confirm this finding. [Cai et al. \(2021\)](#) obtained similar results when comparing to supernova data. Finally, [Castello et al. \(2021\)](#) fitted the ALTB model to supernova and BAO data, together with a distance prior on the CMB. They also found that a local inhomogeneity cannot explain away the Hubble tension. Our analysis improves on previous work by considering subsets of supernova data, a more comprehensive set of observations and by adopting an improved statistical analysis.

This paper is organized as follows. In Section 2 we briefly review the ALTB model and discuss how to estimate the Hubble constant in an inhomogeneous Universe, and in Section 3 we discuss the observations used to constrain the ALTB model. We then show our results in Section 4 and discuss them in Section 5. We conclude in Section 6.

2 AN INHOMOGENEOUS UNIVERSE

In this section, we briefly review the ALTB model. We place the observer at the center of the inhomogeneous region, effectively neglecting anisotropic degrees of freedoms. We also discuss and propose three different ways to compute the Hubble constant in an inhomogeneous but isotropic Universe. Hereafter, we will use the prime to denote a partial derivative with respect to the radial coordinate, r , while the dot will be used to denote a partial derivative with respect to the time coordinate, t . Additionally, we set $c = 1$.

2.1 The ALTB model

The Lemaître–Tolman–Bondi metric (LTB) can be written as (see [Marra et al. 2022](#), for a comprehensive review):

$$ds^2 = -dt^2 + \frac{R'^2(r, t)}{1 + 2r^2 k(r) \tilde{M}^2} dr^2 + R^2(r, t) d\Omega, \quad (2)$$

where $d\Omega = d\theta^2 + \sin^2 \theta d\phi^2$, \tilde{M} is an arbitrary mass scale and $k(r)$ is a free function. The Friedmann–Lemaître–Robertson–Walker metric (FLRW) can be recovered by imposing $k(r) =$

constant and $R(r, t) = a(t)r$, with $a(t)$ being the FLRW scale factor. Besides the curvature profile, $k(r)$, the ALTB model has two more arbitrary functions: the mass function, $m(r)$, and the Big Bang time function, $t_{BB}(r)$. We set these functions following [Camarena et al. \(2022\)](#), that is, we adopt a homogeneous Big Bang time $t_{BB}(r) = 0$ and set the radial coordinate gauge such that $m(r) = 4\pi\tilde{M}^2 r^3/3$. A homogeneous Big Bang time is necessary to ensure the absence of large inhomogeneities at early times, in agreement with the standard paradigm of inflation ([Zibin 2008](#)).

After fixing $m(r)$ and $t_{BB}(r)$, one is left with the curvature function $k(r)$, which we model according to

$$k(r) = k_b + (k_c - k_b)P_3(r/r_B, 0), \quad (3)$$

where k_b and k_c are the curvature outside and at the center of the spherical inhomogeneity, respectively, r_B is the comoving radius of the inhomogeneity and the function $P_n(x)$ follows ([Valkenburg et al. 2014](#)):

$$P_n(x) = \begin{cases} 1 - \exp[-(1-x)^n/x] & 0 \leq x < 1, \\ 0 & 1 \leq x. \end{cases} \quad (4)$$

This curvature profile describes a compensated spherical inhomogeneity, that is, our ALTB model simply becomes a Λ CDM model at $r \geq r_B$. Furthermore, equation (3) establishes the existence of r_L , the compensating scale, at which the central over/underdense region makes a transition to the surrounding mass-compensating under/overdense region.

Due to the radial dependence of $R(r, t)$, the expansion of the universe is not only inhomogeneous but also anisotropic. Then, there exists two scalar factors: the transverse one, $a_{\perp}(r, t) = R(r, t)/r$, and the longitudinal one, $a_{\parallel}(r, t) = R'(r, t)$. This means that there are also two expansion rates defined as

$$H_{\perp}(r, t) = \frac{\dot{a}_{\perp}(r, t)}{a_{\perp}(r, t)}, \quad (5)$$

$$H_{\parallel}(r, t) = \frac{\dot{a}_{\parallel}(r, t)}{a_{\parallel}(r, t)}. \quad (6)$$

Using the previous equations, we can define the present-day density parameters as:

$$\Omega_{\Lambda,0}(r) = \frac{\Lambda}{3H_{\perp}^2(r, t_0)}, \quad (7)$$

$$\Omega_{m,0}(r) = \frac{2m(r)}{R^3(r, t_0)H_{\perp}^2(r, t_0)}, \quad (8)$$

$$\Omega_{k,0}(r) = \frac{2r^2k(r)\tilde{M}^2}{R^2(r, t_0)H_{\perp}^2(r, t_0)}. \quad (9)$$

For the sake of simplicity, hereafter we use $a \equiv a_{\perp}$ and $H \equiv H_{\perp}$, unless otherwise stated.

The matter density contrast is defined by

$$\delta\rho(r, t) = \frac{\rho_m(r, t)}{\rho_m(r_B, t)} - 1, \quad (10)$$

and the mass (integrated) density contrast is given by

$$\begin{aligned} \delta(r, t_0) &= \frac{4\pi \int_0^r d\bar{r} \delta\rho(\bar{r}, t_0) R^2(\bar{r}, t_0) R'(\bar{r}, t_0)}{4\pi R^3(r, t_0)/3} \\ &= \frac{\Omega_{m,0}(r) H_0^2(r)}{\Omega_{m,0}^{\text{out}} H_0^{\text{out}2}} - 1, \end{aligned} \quad (11)$$

where $H_0(r) \equiv H(r, t_0)$. Hereupon, we use the superscript

“out” to denote quantities outside the inhomogeneity, i.e. FLRW background quantities. We additionally define the FLRW comoving coordinate at the present time as:

$$r^{\text{out}} = R(r, t_0)/a^{\text{out}}(t_0). \quad (12)$$

The ALTB model is specified by the parameters that characterize the inhomogeneity, r_B and k_c in equation (3), and by the standard six Λ CDM parameters. The latter are the Hubble constant, the baryon density, the cold dark matter density, the optical depth, the amplitude of the power spectrum, and its tilt. Regarding the ALTB parameters, instead of r_B and k_c , we adopt z_B , which is the redshift corresponding to r_B , and δ_0 , which is the contrast at the center. The motivation for this change of independent variables is that z_B and δ_0 are easier to interpret as far as the low-redshift universe is concerned, the subject of this paper. In the following we will show our results using r_L^{out} , the compensating scale in FLRW comoving coordinates, and $\delta_L \equiv \delta(r_L, t_0)$, the mass density contrast at the aforementioned scale (for illustrative plots, see [Camarena et al. 2022](#)). Finally, in order to improve the convergence of the Monte Carlo Markov Chain (MCMC), we normalize δ_0 such that, instead of $-1 \leq \delta_0 < \infty$, we use:

$$\tilde{\delta}_0 = \begin{cases} \delta_0 & \delta_0 \leq 0 \\ \delta_0/(1 + \delta_0) & \delta_0 > 0 \end{cases}, \quad (13)$$

which satisfies $-1 \leq \tilde{\delta}_0 < 1$. The same normalization is applied for the δ_L . For the sake of simplicity, hereafter we drop the tilde.

2.2 Anisotropies

As said earlier, we consider the observer at the center of a spherical structure, a scenario in which observations are perturbed in a spherically symmetric way. As the universe is both radially inhomogeneous and anisotropic, one may argue that an anisotropic perturbation of observations should be considered. To this point one may consider a more general metric such as the quasi-spherical Szekeres model ([Szekeres 1975](#)), which features a dipole inhomogeneity instead of a spherical one ([Bolejko 2007](#)), or simply displace the observer from the origin ([Alnes & Amarzguoui 2006](#)).

Our modeling, however, is justified *a priori* by the fact that we wish to understand if a local underdensity can explain away the Hubble tension. Indeed, this calls for a 9% increase in the local Hubble rate, which means that the observer must be within a deep underdensity of contrast ≈ -0.5 , see Eq. (1), with subdominant anisotropic corrections. The smaller axis of an underdense ellipsoid grows indeed faster as compared to the longer ones, with the consequence that voids become increasingly spherical as they evolve. If then the observer is misplaced from the center of such a structure, they will develop a peculiar velocity with respect to the CMB of approximately $v = \Delta H d_{\text{obs}}$, where $\Delta H \simeq 6$ km/s/Mpc and d_{obs} is the distance from the center ([Marra & Notari 2011](#)). As the observed CMB dipole is $v/c \simeq 1.2 \times 10^{-3}$ ([Aghanim et al. 2020](#)), this means that $d_{\text{obs}} \lesssim 60$ Mpc, which is small as compared to the size of the inhomogeneity (see Fig. 6): in the standard model a source at $z = 0.15$, the maximum redshift considered in the local H_0 determination by SH0ES, is at a distance of ≈ 600 Mpc.

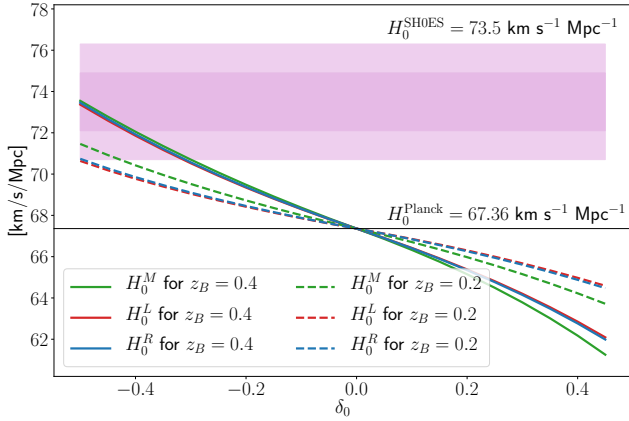


Figure 1. H_0^M , H_0^R and H_0^L as a function of the central contrast δ_0 for $z_B = 0.2$ and $z_B = 0.4$. A local void with $\delta_0 \approx -0.5$ and $z_B = 0.2$ or $\delta_0 \approx -0.3$ and $z_B = 0.4$ can potentially solve the Hubble crisis by providing a background expansion $H_0^{\text{out}} = H_0^{\text{Planck}}$ (horizontal black line) and a local rate that agrees with H_0^{SH0ES} (pink region).

We conclude that our modeling is adequate for testing the local-void scenario. On the other hand, it is worth stressing that the local-void scenario fine-tunes the position of the observer by $\approx (60/600)^3 = 1/1000$ chances. In other words, if successful, one trades a one-in-a-million (5σ) inconsistency in data with a one-in-a-thousand fine-tuning.

2.3 The Hubble constant

Although the background FLRW expansion is well defined by the value of H_0^{out} , due to the radial dependency on the expansion rate, $H_0(r) \neq \text{constant}$, our model does not possess a unique definition of the Hubble constant. In addition, there does not exist, *a priori*, any preferable scale, r_x , at which one can safely define $H_0 = H_0(r_x)$ – the definition of the Hubble constant remains arbitrary.

Here, we use observational reasoning and extend FLRW concepts to propose three definitions of the Hubble constant for a ALTB universe. These approaches use a mock catalog of supernovae in the redshift range $0.023 < z < 0.15$, which is generated considering ALTB luminosity distances as the observed quantity, and the redshift distribution and covariance matrix of the Pantheon dataset (Scolnic et al. 2018). This mock data set is generated at each sampled point of the parameter space in order to correctly account for the different cosmological model and it is used only for the determination of the predicted Hubble constant.

2.3.1 Mean Hubble constant H_0^M

Our first approach, dubbed as H_0^M , is an extension of the one proposed in Valkenburg et al. (2014). H_0^M is obtained from a weighted comparison between the luminosity distance and a radial dependent cosmographic expansion over the range $0.023 < z < 0.15$:

$$\frac{c}{H_0^M} = \int_{0.023}^{0.15} d_L(z) W(z) \left\{ z + \frac{1}{2} [1 - q_0(r)] z^2 \right\}^{-1} dz, \quad (14)$$

where $W(z)$ is the normalized redshift distribution of the mock supernovae and the deceleration parameter is defined as

$$q_0(r) = \Omega_{m,0}(r)/2 - \Omega_{\Lambda,0}(r). \quad (15)$$

2.3.2 SH0ES Hubble constant H_0^R

For our second definition we adopt the procedure proposed in Redlich et al. (2014), and lately in Efstathiou (2021), where the Hubble constant is obtained by mimicking the typical cosmic distance ladder procedure (see for instance Riess et al. 2016), i.e., fitting the mock catalog using the FLRW cosmographic expansion and assuming a constant deceleration parameter $q_0 = -0.55$ along with a constant value for H_0 . This determination, dubbed H_0^R , neglects any spatial degrees of freedom introduced by the LTB metric and it could be used to identify if deviations of statistical homogeneity could substantially bias cosmic distance ladder determinations. We would like to stress that, while Redlich et al. (2014) first presented this method in the context of inhomogeneous models, Efstathiou (2021) proposed this approach to point out that the cosmic distance ladder technique does not determine the Hubble rate at $z = 0$ but in a specific low- z range given by the set of supernovae that is adopted in the cosmic distance ladder.

2.3.3 Local Hubble constant H_0^L

Lastly, we propose H_0^L , which is determined as H_0^R but with a radial dependent deceleration parameter:

$$\tilde{q}_0(r, H_0^L) = q_0(r) \left[\frac{H_0(r)}{H_0^L} \right]^2, \quad (16)$$

where the last factor enforces the constant H_0^L as the local Hubble rate when defining the density parameters of equations (7-8).

Figure 1 shows H_0^M , H_0^R and H_0^L as a function of δ_0 for two particular values of the boundary redshift: $z_B = 0.2$ (dashed lines) and $z_B = 0.4$ (solid lines). One can note that H_0^R (blue lines) and H_0^L (red lines) provide similar values for any pair of δ_0 and z_B . On the other hand, H_0^M (green lines) enhances the deviations from H_0^{out} , especially at $|\delta_0| \gtrsim 0.1$. A local void with $\delta_0 \approx -0.5$ and $z_B = 0.2$ or $\delta_0 \approx -0.3$ and $z_B = 0.4$ can potentially solve the Hubble crisis by providing a background expansion in agreement with the CMB, $H_0^{\text{out}} = H_0^{\text{Planck}}$, and a local rate that agrees with SH0ES.

3 OBSERVABLES

In order to constrain the ALTB model we use: Planck 2018 data coming from the high- ℓ and low- ℓ TT+TE+EE power spectrum (Aghanim et al. 2018); BAO measurements from 6dFGS (Beutler et al. 2011), SDSS-MGS (Ross et al. 2015) and BOSS-DR12 (Alam et al. 2017); cosmic chronometers data from Moresco et al. (2016, 2012); Simon et al. (2005); Stern et al. (2010); Zhang et al. (2014); Moresco (2015);¹

¹ See Moresco et al. (2022) for the most recent compilation.

type Ia supernovae distances from Pantheon compilation (Scolnic et al. 2018); a 2σ upper limit prior on the Compton y -distortion provided by COBE-FIRAS (Fixsen et al. 1996); a prior on the amplitude of kSZ effect at $\ell = 3000$ (Reichardt et al. 2020); and the Cepheid calibration of the absolute magnitude of supernovae, M_B , from Camarena & Marra (2020, 2021). See Camarena et al. (2022) for a thorough discussion of this data and its ALTB theoretical description.

We will carry out our analyses using several combinations of the aforementioned data. Moreover, we will also consider combinations of data including not the whole set of Pantheon supernovae but only supernovae in the redshift range $0.023 < z < 0.15$ —the so-called Hubble flow supernovae that are used by SH0ES in the determination of H_0 . We dub this subset of the Pantheon catalog as low- z supernovae. Additionally, we carried out analyses including a prior on the Hubble constant, instead of a prior on M_B . Specifically, we impose the SH0ES determination $H_0 = 73.5 \pm 1.4 \text{ km s}^{-1} \text{ Mpc}^{-1}$ (Reid et al. 2019) on H_0^L . The aim of these extra analyses is to demonstrate that both methods, either with a prior on M_B or a prior on H_0 , are statistically equivalent when the local H_0 prior is implemented considering that the cosmic distance ladder technique does not measure the Hubble rate at $z = 0$ but rather in a specific redshift range (Efstathiou 2021).

4 RESULTS

Data analysis is performed using the MONTELLTB code (Camarena et al. 2022), which conveniently wraps a modified version of the ALTB solver VD2020 (Valkenburg 2012) in MONTEPYTHON (Brinckmann & Lesgourgues 2018; Audren et al. 2013). We explore via MCMC the parameter space, and evaluate the convergence of our chains demanding $(R - 1) \lesssim 0.05$ for the inhomogeneous parameters and $(R - 1) \sim \mathcal{O}(10^{-3})$ for the Λ CDM background parameters, where R is the Gelman-Rubin diagnostic (Gelman & Rubin 1992). Most of the plots displayed in this section were generated using GETDIST (Lewis 2019).

We extend the assumptions made in Camarena et al. (2022) and consider both a flat and a curved Λ CDM background. Given that Planck data has showed a moderate evidence for a closed Universe (Di Valentino et al. 2019; Handley 2021), the question if our Universe is flat or curved has been recently investigated (see, e.g., Vagnozzi et al. 2021b,a). Additionally, the FLRW curvature has been found to have a strong correlation with a possible change in the CMB temperature, potentially pointing out the existence of a strong correlation with the parameters of an inhomogeneous model (Bose & Lombriser 2021; Ivanov et al. 2020).

As mentioned before, we considered several combinations of the data discussed in Section 3. We denote as Base the combination of CMB, SNe and the local prior (either on H_0 or M_B). We quantify the tension on H_0 and M_B assuming the one-dimensional Gaussian limit of the index of inconsistency; a moment-based estimator that can be used to quantitatively measure discordance (Lin & Ishak 2017).

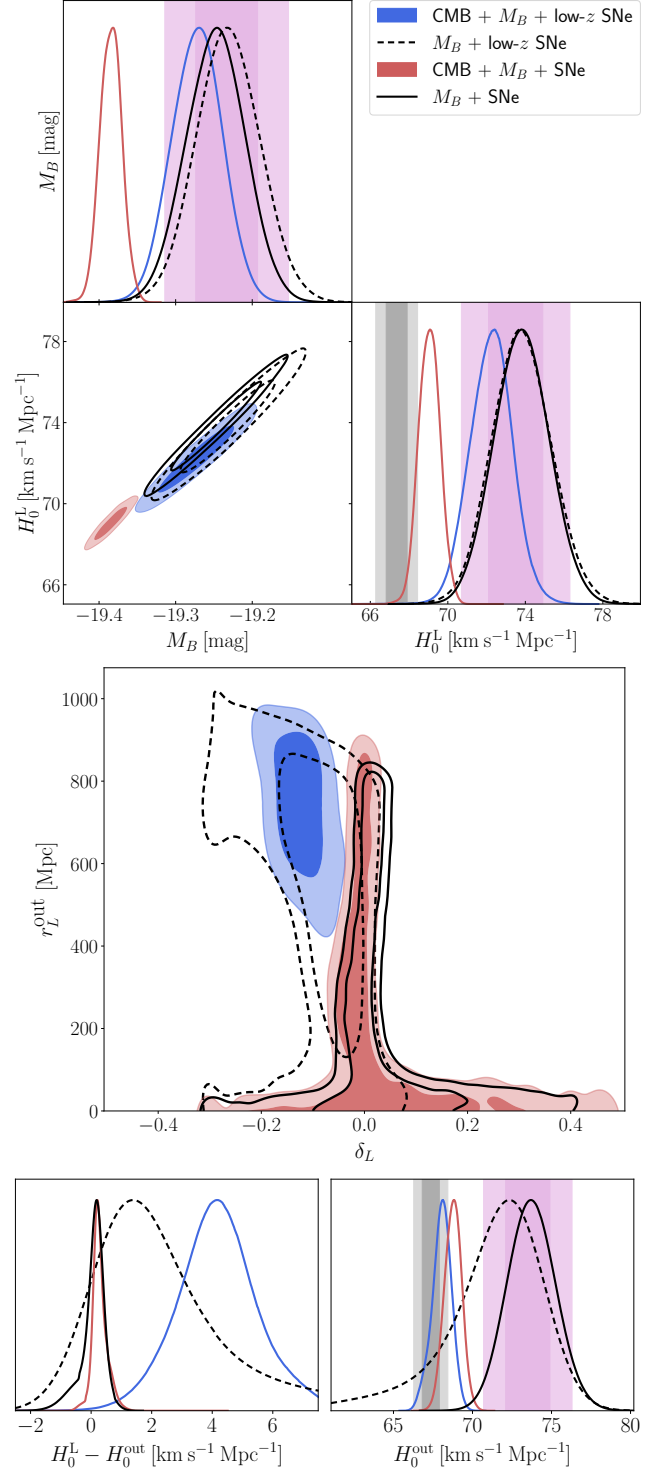


Figure 2. Marginalized constraints, at 68% and 95% confidence level, on several parameters of interest when considering, in a flat background Universe, combinations of CMB and supernova data, together with the local prior on the supernova absolute magnitude M_B . Shown are M_B and the local Hubble rate H_0^L (top), the effective mass density contrast δ_L and compensating scale r_L^{out} of the ALTB model (center), and background Hubble constant H_0^{out} and the local increase with respect to the background rate, $\Delta H = H_0^L - H_0^{\text{out}}$ (bottom). Note that there is tension only when considering all supernovae and the CMB. See Section 4.1.

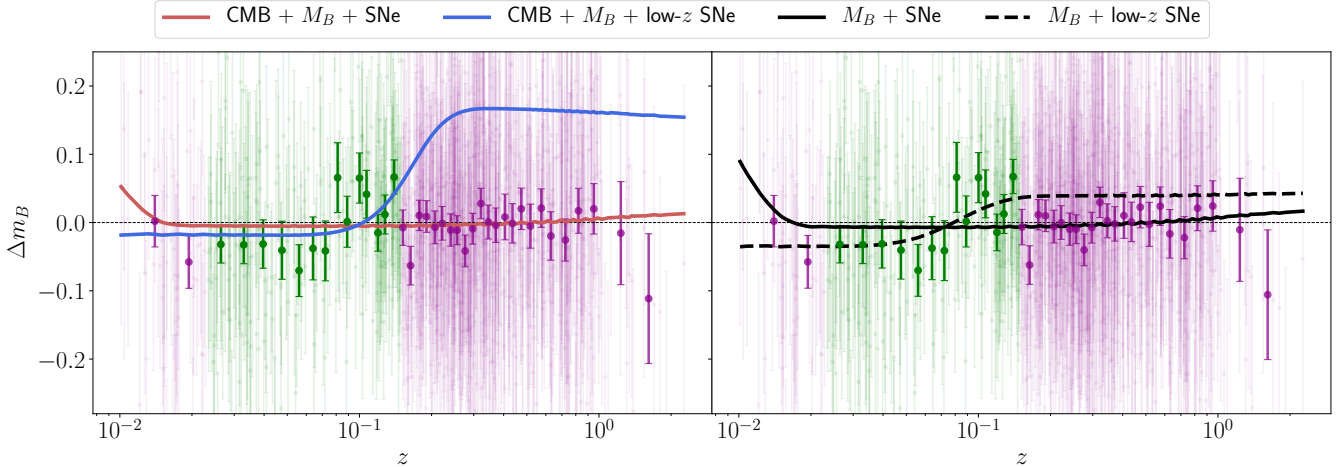


Figure 3. Apparent magnitude residuals of the Pantheon supernovae, as function of the redshift, taking as a reference the best fit of the Λ CDM model to the combination CMB + M_B + SNe + All. One can see, from the left panel, that the best fit of the ALTB model to CMB + M_B + low- z SNe (blue line) fits well the supernovae in the range $0.023 < z < 0.15$ (green data points) and provides a solution to the Hubble crisis, see Section 4.1. However, the other supernovae (purple data points) constrain the ALTB luminosity distance (red line) to a shape similar to the Λ CDM one. The result is that the ALTB model cannot explain the Hubble tension. The right panel shows the case without CMB data. While the full supernova sample does not prefer an underdensity (solid curve), when only considering low- z supernovae one sees that the profile is compatible with a local void (dashed black line). This is due to a fluctuation in the supernova apparent magnitudes at $0.1 \lesssim z \lesssim 0.15$.

4.1 Flat background FLRW metric

We start by considering a flat Λ CDM background ($\Omega_k^{\text{out}} = 0$) and only CMB and supernova observations, together with the local prior on the supernova absolute magnitude M_B . Figure 2 shows marginalized constraints on several parameters of interest for four observable combinations.² Figure 3 shows the corresponding apparent magnitude residuals of the ALTB best fits with respect to the Λ CDM best fit.

As it is well known, the freedom in defining the LTB curvature function allows one to fit any luminosity-distance-redshift relation, that is, any supernova sample. If one adds a prior on M_B , then the latter simply constrains the supernova absolute magnitude, and so local H_0 , without changing the fit to supernova data. We start by discussing this case for the full Pantheon sample and its low-redshift subset ($0.023 < z < 0.15$). From Figure 2 we see that the constraints on δ_L and r_L^{out} from the full SN sample (solid black lines) are along the $\delta_L = 0$ axis, not favoring under- or overdensities. In particular, one has $H_0^L \approx H_0^{\text{out}} \approx H_0^{\text{SHOES}}$. In other words, there is no local void nor H_0 tension, as expected.

If one considers only low- z supernovae (dashed black lines), the situation is qualitatively the same, albeit with weaker constraints. Note, however, that a local underdensity is somewhat preferred: this is caused by a fluctuations in the supernova apparent magnitudes at $0.1 \lesssim z \lesssim 0.15$, as evident from Figure 3. Because of this allegedly random fluctuation, there is a small shift between H_0^L and H_0^{out} , see Figure 2.

Next we add CMB observations, which are fit by a lower background H_0 as compared with H_0^{SHOES} . If we consider

low- z supernovae (blue curves), then one can have all the supernovae inside a local underdensity and is free to fit any $\Delta H = H_0^L - H_0^{\text{out}}$, see Figures 2 and 3. Specifically, the data favors a local underdensity and the local value of the Hubble rate is in agreement with the local prior and the tension between CMB observations and the local prior is solved. Note also that the local calibration of M_B is not affected by CMB observations. Table 1 shows the marginalized constraints for the relevant parameters, including H_0^L , H_0^R , and H_0^M . We also show the change in the observed CMB temperature $\Delta T \equiv T_0^{\text{obs}} - T_0^{\text{out}}$, with T_0^{obs} being the CMB temperature measured by the observer and $T_0^{\text{out}} = 2.7255$ K the background temperature.³ Indeed, analogous to other parameters, the observer at the center of the inhomogeneity is expected to measure a different CMB temperature as compared with the expected FLRW background temperature. This change in the temperature is strongly related to the features of the inhomogeneity. Within this scenario one expects a ≈ 2 mK change in the CMB temperature. It is worth pointing out that the fact that the analysis M_B + low- z SNe also suggests a similar underdensity is a coincidence: even without the fluctuation at $0.1 \lesssim z \lesssim 0.15$ one would have obtained here a similar result.

Then, we consider the full Pantheon sample. In this case, the luminosity-distance-redshift relation mapped by the supernovae does not allow for a sufficiently large and deep underdensity that can solve the H_0 tension: a sudden change in the luminosity distance is not allowed by the supernovae at $z > 0.15$, see Figures 2 and 3. In particular, CMB data induce a lower value of M_B , at odds with the local prior, the so-called M_B tension (Camarena & Marra

² See Appendix A for the plot relative to the case with the local prior on H_0 .

³ Note that we have neglected possible dynamical effects of radiation (Clarkson & Regis 2011)

2021). Also, in this case, the change in the CMB temperature is much smaller, approximately ≈ 0.01 mK. Our results are that a local void is not favored by the data and the H_0 tension is not solved. Note, however, that $\Delta H = H_0^L - H_0^{\text{out}}$ does prefer small but positive values, that is, and underdensity. We will come back to this in Section 5.3.

Finally, we include other observables, considering all the combinations discussed in Camarena et al. (2022). Table 1 presents the relevant results, including the corresponding χ_{min}^2 and the resulting tensions on M_B and H_0 , with respect to Camarena & Marra (2020) and Reid et al. (2019), respectively.

4.2 Curved background FLRW metric

We also study the case of a non-flat FLRW background. Results for these analyses are shown in Table 2 and Figure 4. From Table 2, we can see that the inclusion of the curvature does not significantly change the overall results. In particular, the data favors a slightly open universe with $\Omega_{k,0} \approx 0.002$, compatible with the flat case at 2σ . In particular, in Figure 4 we do not observe a strong correlation between $\Omega_{k,0}$ and the other parameters, in particular ΔT , which remains constrained around zero.

Finally, Figure 5 shows the different values obtained for H_0^L and M_B for our different analyses, both considering a prior on M_B and H_0 . For the sake of the comparison, we have also included the results coming from analyses of the Λ CDM model. We can see how the ALTB results follow the ones relative to the Λ CDM model.

5 DISCUSSION

5.1 Model selection

We have seen how the Hubble tension is solved when only low-redshift supernovae are considered but it is no longer solved when all supernovae are included. Here, we will quantify this statement using Bayesian model comparison between the Λ CDM and ALTB models. We perform model selection using the Bayes ratio. Since the Λ CDM model is nested in the ALTB model, we can simplify the computation of the Bayes ratio by using the Savage-Dickey density ratio (SDRR) (Trotta 2008). This technique reduces the Bayes ratio to:

$$B_{01} = \frac{\int \mathcal{P}(\delta_0, z_B, \theta_i) d\theta_i}{p(\delta_0)p(z_B)} \Bigg|_{\delta_0=0, z_B=0}, \quad (17)$$

with \mathcal{P} being the posterior of the ALTB model, θ_i the Λ CDM background parameters, and p the prior function. Although the SDRR can be safely applied to nested models, one should bear in mind that equation (17) assumes that priors are separable, i.e., $p(\delta_0, z_B, \theta_i) = p(\delta_0)p(z_B)p(\theta_i)$. Here, this assumption is fully satisfied since our analyses use wide flat priors over all parameters.⁴ Specifically, we impose $z_B \in [0, 0.5]$ and $\delta_0 \in [-1, 1]$ such that the flat priors result in $p(\delta_0) = 1/2$ and $p(z_B) = 2$. In equation (17)

it is $B_{01} \propto \mathcal{E}_0/\mathcal{E}_1$, with 0 representing the nested model, in our case the Λ CDM model, and 1 the more complex model, the ALTB model. We qualitatively interpret the ratio B_{01} via the Jeffreys' scale (Jeffreys 1961). Specifically, we adopt the conservative version discussed in Trotta (2008), see Table B1.

We also use the Akaike information criterion (AIC):

$$\text{AIC} = \chi_{\text{min}}^2 + 2k, \quad (18)$$

with k being the number of free parameters. The relative differences $\Delta\text{AIC} \equiv \text{AIC}_{\text{ALTB}} - \text{AIC}_{\Lambda\text{CDM}}$ are qualitatively interpreted using the calibrated Jeffreys' scale shown in Table B2.

Results are shown in Tables 3 and 4 for the flat and curved Λ CDM background, respectively. Under the assumption of a flat background metric, we find a strong evidence, $B_{01} = -12.5$, in favor of the ALTB model when the CMB + M_B + low- z SNe data is considered. This is confirmed by the ΔAIC which shows no support to the Λ CDM model. On the other hand, the inclusion of the full supernova dataset removes the preference for the ALTB model. The analysis relative to the combination CMB + M_B + All shows a moderate evidence for the Λ CDM model, $B_{01} = 3.0$, and a substantial support to the same model, $\Delta\text{AIC} = 2.2$. Similar results are obtained by considering a prior on H_0 . Finally, as can be seen from Table 4, the introduction of a non-vanishing background curvature does not qualitatively change the results discussed above.

5.2 Generalized curvature profile

As discussed in Section 2, the ALTB model has three arbitrary functions. We have set two of them, $m(r)$ and $t_{BB}(r)$, using a gauge choice and physical arguments. On the other hand, our particular choice of $k(r)$ is still arbitrary. Here, we study the impact, on the Hubble tension problem, of such an assumption by performing an extra analysis that uses a generalization of equation (3):

$$P_3(x, \alpha) = \begin{cases} 1 & \text{for } 0 \leq x < \alpha \\ 1 - \exp\left[\frac{1-\alpha}{x-\alpha}\left(\frac{x-\alpha}{1-\alpha} - 1\right)^3\right] & \text{for } \alpha \leq x < 1, \\ 0 & \text{for } 1 \leq x \end{cases}, \quad (19)$$

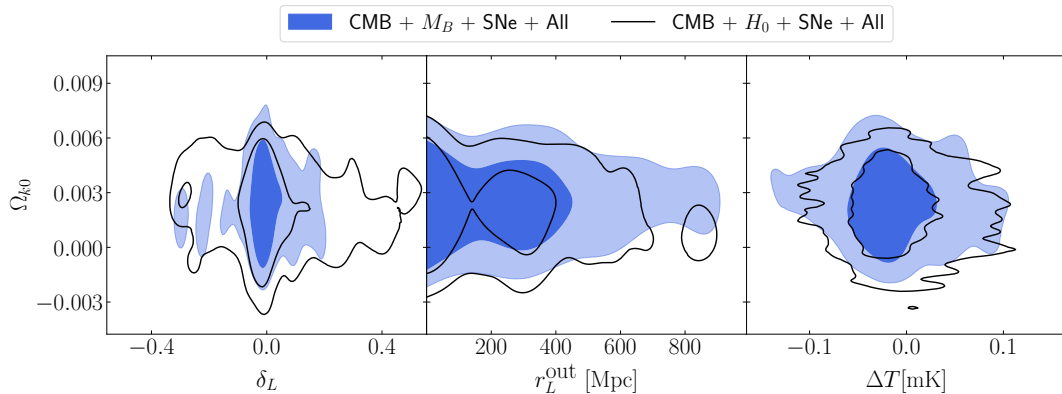
where $0 < \alpha < 1$ is a new parameter that modifies the smoothness of the transition between the inner and background regions. Sharper profiles are obtained when α approximates unity. Note that our main analysis with equation (3) can be recovered by setting $\alpha = 0$.

Results are shown in Table 5, where, for the sake of comparison, we also report the results relative to $\alpha = 0$. The addition of the parameter α leads to an increase in the value of H_0^L by $0.64 \text{ km s}^{-1} \text{ Mpc}^{-1}$ as compared with the previous analysis with $\alpha = 0$. This, along with the increment on the error, reduces the Hubble tension to 2.7σ . The tension on M_B decrease to 3.2σ . In other words, we find a small improvement with respect to the analysis, but the ALTB cannot fully explain the tension. The assumption of the generalized curvature profile of equation (19) reduces the χ_{min}^2 by 0.3 so that we obtain $\Delta\text{AIC} = 1.7$ and $B_{01} = 1.9$ in favor of the simplest model with $\alpha = 0$. Namely, a weak evi-

⁴ Except for H_0^L and M_B , but the priors are still separable.

Table 1. 68% confidence level intervals for the relevant parameters for the different combinations of data here analyzed, considering both the prior on H_0 and M_B . We also report the χ^2_{\min} and the tensions on H_0 and M_B in sigma units.

Parameter	CMB + loc. prior + low- z SNe	Base	Base + BAO + Hz	Base + y -dist.	Base + kSZ	Base + All
Prior on M_B						
M_B [mag]	$-19.271^{+0.032}_{-0.035}$	$-19.384^{+0.014}_{-0.014}$	$-19.389^{+0.011}_{-0.012}$	$-19.386^{+0.014}_{-0.014}$	$-19.384^{+0.014}_{-0.014}$	$-19.391^{+0.012}_{-0.012}$
H_0^M [km/s/Mpc]	$72.47^{+1.09}_{-1.10}$	$69.06^{+0.53}_{-0.60}$	$68.89^{+0.44}_{-0.46}$	$69.01^{+0.58}_{-0.55}$	$69.07^{+0.56}_{-0.54}$	$68.77^{+0.40}_{-0.46}$
H_0^L [km/s/Mpc]	$72.29^{+1.11}_{-1.12}$	$69.06^{+0.54}_{-0.57}$	$68.89^{+0.43}_{-0.46}$	$69.00^{+0.57}_{-0.53}$	$69.07^{+0.55}_{-0.54}$	$68.78^{+0.39}_{-0.44}$
H_0^R [km/s/Mpc]	$72.38^{+1.12}_{-1.14}$	$69.06^{+0.52}_{-0.54}$	$68.90^{+0.41}_{-0.44}$	$69.00^{+0.54}_{-0.54}$	$69.07^{+0.53}_{-0.50}$	$68.79^{+0.37}_{-0.42}$
ΔT [mK]	$1.861^{+0.639}_{-0.918}$	$-0.017^{+0.042}_{-0.041}$	$-0.007^{+0.027}_{-0.045}$	$-0.009^{+0.025}_{-0.048}$	$-0.023^{+0.023}_{-0.027}$	$-0.022^{+0.022}_{-0.025}$
Tension on H_0	0.7	3.0	3.1	3.0	2.9	3.2
Tension on M_B	0.7	3.5	3.7	3.6	3.5	3.8
χ^2_{\min}	2996.1	3808.7	3826.7	3807.3	3808.0	3828.2
Prior on H_0						
M_B [mag]	$-19.258^{+0.047}_{-0.044}$	$-19.386^{+0.015}_{-0.015}$	$-19.391^{+0.012}_{-0.012}$	$-19.389^{+0.015}_{-0.015}$	$-19.389^{+0.014}_{-0.014}$	$-19.392^{+0.011}_{-0.012}$
H_0^M [km/s/Mpc]	$73.01^{+1.49}_{-1.53}$	$69.09^{+0.56}_{-0.58}$	$68.90^{+0.47}_{-0.49}$	$68.98^{+0.59}_{-0.60}$	$68.94^{+0.55}_{-0.51}$	$68.83^{+0.43}_{-0.46}$
H_0^L [km/s/Mpc]	$72.83^{+1.53}_{-1.49}$	$69.08^{+0.57}_{-0.56}$	$68.88^{+0.44}_{-0.47}$	$68.97^{+0.55}_{-0.58}$	$68.94^{+0.54}_{-0.51}$	$68.83^{+0.41}_{-0.44}$
H_0^R [km/s/Mpc]	$72.94^{+1.56}_{-1.51}$	$69.08^{+0.54}_{-0.53}$	$68.89^{+0.46}_{-0.46}$	$68.98^{+0.54}_{-0.55}$	$68.94^{+0.51}_{-0.48}$	$68.84^{+0.39}_{-0.42}$
ΔT [mK]	$2.145^{+0.869}_{-1.043}$	$0.004^{+0.021}_{-0.065}$	$0.007^{+0.024}_{-0.061}$	$0.001^{+0.056}_{-0.067}$	$-0.017^{+0.026}_{-0.032}$	$-0.015^{+0.020}_{-0.036}$
Tension on H_0	0.3	2.9	3.1	3.0	3.0	3.2
Tension on M_B	0.4	3.6	3.8	3.6	3.6	3.8
χ^2_{\min}	2998.3	3803.8	3826.8	3805.0	3803.0	3824.5

**Figure 4.** Marginalized constraints on the effective mass density contrast δ_L , compensating scale r_L^{out} , temperature deviation ΔT and background curvature $\Omega_{k,0}$ at 68% and 95% confidence levels.

dence in favor of the curvature profile given by equation (3) is found.

5.3 Mapping the local structure of the universe

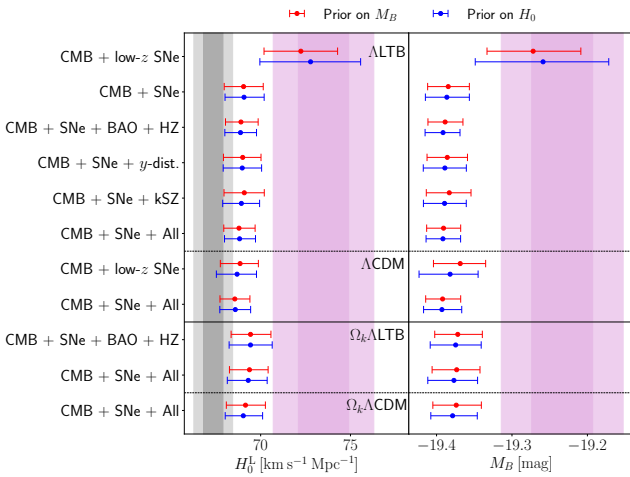
While Occam's razor favors the Λ LTB model with $\alpha = 0$, the generalized curvature profile is useful to map the local matter distribution. Figure 6 shows the rates of expansion $H_{\parallel}(r, t_0)$ and $H_{\perp}(r, t_0)$ (right panel), the matter and mass density (top mid panel), and the deviations of $\Omega_{m,0}$ and $\Omega_{k,0}$

from the Λ CDM background (bottom mid panel) as functions of the comoving FLRW coordinate r^{out} for the best fit of the analysis CMB + M_B + All with equation (19) (solid lines). Local fluctuations in the matter density parameters were found by Colgáin et al. (2022) when analyzing supernova data. We also display the same quantities considering the best fit of our main analysis with $\alpha = 0$ (dashed lines). The best-fit values are

$$\{\alpha, \delta_L, r_L^{\text{out}}, \Omega_{m,0}^{\text{out}}, H_0^{\text{out}}\} = \{0.28, -0.038, 330, 0.304, 68.3\} \quad (20)$$

Table 2. As Table 1, but for a curved background, $\Omega_{k,0} \neq 0$.

Parameter	Base + BAO + Hz	Base + All
Prior on M_B		
Ω_{k0}	$0.0024^{+0.0016}_{-0.0016}$	$0.0024^{+0.0017}_{-0.0017}$
M_B [mag]	$-19.372^{+0.016}_{-0.016}$	$-19.373^{+0.017}_{-0.015}$
H_0^M [km/s/Mpc]	$69.41^{+0.59}_{-0.61}$	$69.38^{+0.62}_{-0.55}$
H_0^L [km/s/Mpc]	$69.42^{+0.58}_{-0.59}$	$69.38^{+0.61}_{-0.53}$
H_0^R [km/s/Mpc]	$69.42^{+0.56}_{-0.58}$	$69.39^{+0.59}_{-0.52}$
ΔT [mK]	$-0.016^{+0.026}_{-0.039}$	$-0.020^{+0.020}_{-0.032}$
Tension on H_0	2.7	2.7
Tension on M_B	3.2	3.2
χ^2_{\min}	3828.4	3829.0
Prior on H_0		
Ω_{k0}	$0.0022^{+0.0017}_{-0.0017}$	$0.0021^{+0.0018}_{-0.0017}$
M_B [mag]	$-19.375^{+0.017}_{-0.017}$	$-19.377^{+0.018}_{-0.015}$
H_0^M [km/s/Mpc]	$69.43^{+0.61}_{-0.65}$	$69.30^{+0.60}_{-0.57}$
H_0^L [km/s/Mpc]	$69.41^{+0.59}_{-0.62}$	$69.30^{+0.57}_{-0.56}$
H_0^R [km/s/Mpc]	$69.43^{+0.58}_{-0.61}$	$69.31^{+0.57}_{-0.55}$
ΔT [mK]	$0.004^{+0.028}_{-0.060}$	$-0.014^{+0.016}_{-0.032}$
Tension on H_0	2.7	2.8
Tension on M_B	3.2	3.3
χ^2_{\min}	3820.1	3822.7


Figure 5. Constraints on H_0^L and M_B at 95% confidence level for the cases here considered. The gray area corresponds to the value of the Hubble constant at 68% and 95% confidence level inferred from the CMB observations (Aghanim et al. 2018), while the pink areas correspond to the H_0 determination by SH0ES (Reid et al. 2019) and the corresponding calibration of M_B (Camarena & Marra 2020).

for the case of the generalized profile of equation (19), and $\{\delta_L, r_L^{\text{out}}, \Omega_{m,0}^{\text{out}}, H_0^{\text{out}}\} = \{-0.013, 294, 0.302, 68.4\}$ (21)

for the case with $\alpha = 0$.

The left panel of Figure 6 shows size r_L^{out} and depth δ_L of the two best-fit models as compared with the standard model expectation, which is quantified via the Copernican prior convolved with the CMB likelihood (see Camarena et al. 2022). We can see that the data prefers a shallow void with $\delta_L \approx -0.04$ and $r_L^{\text{out}} \approx 300$ Mpc, which, interestingly, lies on the border of the 95% credible region relative to the standard model expectation.

Even though the analysis including α allows us to map the local distribution of matter in a more general way, the local structure of the Universe could be restricted using a yet more general profile, such as an n -node spline function (Redlich et al. 2014) or a data-driven technique, possibly including anisotropic degrees of freedom. Indeed, while our modeling is adequate to test if a local underdensity can explain away the Hubble tension, see Section 2.2, it may be important to consider anisotropies when modeling a shallow structure such as the one depicted in Figure 6. This is also suggested by recent maps of our cosmological neighborhood (Courtois et al. 2013). We leave this problem to the future.

6 CONCLUSIONS

In Camarena et al. (2022), we pursued a program to test one of the fundamental assumptions of modern cosmology: the Copernican principle. In particular, we modeled the space-time around us without any prior on the parameters that describe the inhomogeneity, but rather letting observations constrain the local structure. Our analysis showed that current cosmological data can tightly constrain radial deviations from the FLRW metric at almost the cosmic variance level. We also showed that typical constraints on the Λ CDM parameters are not weakened if one drops the Copernican hypothesis. Here, our aim was to quantify the impact of the Copernican principle on the Hubble problem: can a non-Copernican structure explain away the Hubble tension?

In order to robustly answer this question, we put care on how to compute the Hubble constant in a inhomogeneous universe, which we parametrize via the ALT model—basically a radial perturbation of a FLRW metric. We adopted three different definitions, which all give basically similar results. Then, in order to quantitatively conclude if the extra geometrical degrees of freedom of the ALT model are favored by the data, we carried out Bayesian model selection via both the Bayes factor and the Akaike information criterion. Finally, we considered both a flat and a curved background FLRW model. Our results show that the ALT model can successfully explain away the H_0 tension and is favored with respect to the Λ CDM model only if one solely considers supernovae in the redshift range that is used to fit the Hubble constant, that is, $0.023 < z < 0.15$. If one considers all the supernova sample then the H_0 tension is not solved and the support for the ALT model vanishes. We have also carried out an analysis that adopts a more general curvature profile. We have found that the inclusion of a new parameter, that sharpen or smooth the transition between the inner inhomogeneity and the background model, does

Table 3. Results of the model selection analysis for the case of a flat background Universe ($\Delta x = x_{\text{ALTB}} - x_{\Lambda\text{CDM}}$).

Criteria	CMB + M_B + low- z SNe	CMB + H_0 + low- z SNe	CMB + M_B + All	CMB + H_0 + All
$\chi^2_{\Lambda\text{CDM}}$	3014.3	3015.0	3830.0	3825.2
$\Delta\chi^2$	-18.2	-16.7	-1.8	-0.7
ΔAIC	-14.2	-12.7	2.2	3.3
$\ln B_{01}$	-12.5	-17.3	3.0	2.2

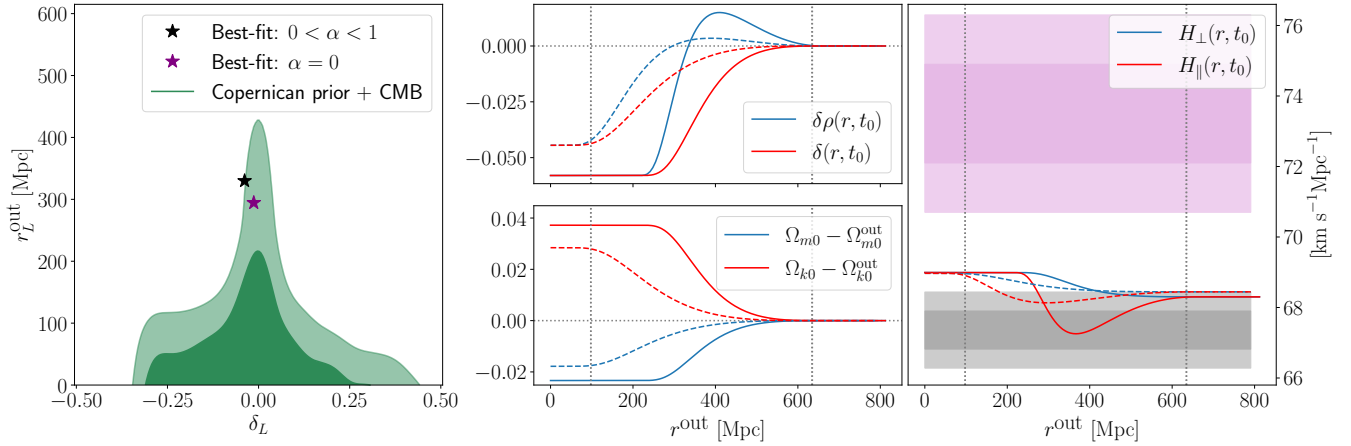

Figure 6. Characterization of our local spacetime from the best fit to all data of the ALTb analysis with the generalized profile with $0 < \alpha < 1$ (solid lines) and with $\alpha = 0$ (dashed lines). The panel on the left shows the size r_L^{out} and depth δ_L of the two best-fit models as compared with the standard model expectation, which is quantified via the Copernican prior convolved with the CMB likelihood (see Camarena et al. 2022). The panels in the middle show the matter and mass density contrasts (top) and the deviations of $\Omega_{m,0}$ and $\Omega_{k,0}$ from the ΛCDM background (bottom) as functions of the comoving FLRW coordinate r^{out} . The dotted vertical lines mark the redshift range $0.023 < z < 0.15$ that is used to determine H_0 . The panel on the right shows the rates of expansion $H_{\parallel}(r, t_0)$ and $H_{\perp}(r, t_0)$ a function of r^{out} . The purple and gray areas correspond to constraints at 68% and 95% confidence level of the Hubble constant as determined by the SH0ES (Reid et al. 2019) and Planck collaboration (Aghanim et al. 2018), respectively. See Section 5.3 for details.

Table 4. Results of the model selection analysis for the case of a curved background Universe ($\Delta x = x_{\text{ALTb}} - x_{\Lambda\text{CDM}}$).

Criteria	CMB + M_B + All	CMB + H_0 + All
$\chi^2_{\Lambda\text{CDM}}$	3828.7	3824.9
$\Delta\chi^2$	0.4	-2.2
ΔAIC	4.4	1.8
$\ln B_{01}$	2.2	2.4

Table 5. 68% confidence level intervals for the relevant parameters. See Section 5.2 for details.

Parameter	α free	$\alpha = 0$
M_B	$-19.372^{+0.016}_{-0.016}$	$-19.391^{+0.012}_{-0.012}$
H_0^M	$69.41^{+0.59}_{-0.61}$	$68.77^{+0.40}_{-0.46}$
H_0^L	$69.42^{+0.58}_{-0.59}$	$68.78^{+0.39}_{-0.44}$
H_0^R	$69.42^{+0.56}_{-0.58}$	$68.79^{+0.37}_{-0.42}$
$\Delta T[\text{mK}]$	$-0.016^{+0.026}_{-0.039}$	$-0.022^{+0.022}_{-0.025}$
Tension H_0	2.7	3.2
Tension M_B	3.2	3.8
χ^2_{min}	3827.9	3828.2

not provide a solution to the Hubble constant problem, only slightly increasing the local expansion rate. Our results are in good agreement with previous studies and improve upon them by considering a thorougher statistical analysis and a more comprehensive set of observations.

Finally, we have used the generalized curvature profile to reconstruct our local spacetime. We have found that the best fit to current cosmological data corresponds to a shallow void with $\delta_L \approx -0.04$ and $r_L^{\text{out}} \approx 300$ Mpc, which, interestingly, lies on the border of the 95% credible region relative to the standard model expectation. A more generic reconstruction of the local matter distribution of the Universe could be achieved using data-driven methods. We leave the study of this topic for future research.

ACKNOWLEDGMENTS

It is a pleasure to thank Wessel Valkenburg for sharing VoidDistances2020. DC thanks CAPES for financial support. VM thanks CNPq and FAPES for partial financial support. CC is supported by the UK Science & Technology Facilities Council Consolidated Grant ST/P000592/1. This work made use of the CHE cluster, managed and funded by COSMO/CBPF/MCTI, with financial support from FINEP and FAPERJ, and operating at the Javier Magnin Computing Center/CBPF. This work also made use of the Virgo

Cluster at Cosmo-ufes/UFES, which is funded by FAPES and administrated by Renan Alves de Oliveira.

AUTHOR CONTRIBUTIONS

VM and CC conceived the research question. All authors designed the study and analysis plan. DC led the numerical implementation of the model and observables and the MCMC exploration. ZS contributed to the numerical implementation and MCMC exploration. DC and VM drafted the initial version of the manuscript. All authors critically reviewed early and final versions of the manuscript.

DATA AVAILABILITY

The data underlying this article will be shared on reasonable request to the corresponding author. The `monteLLTB` code is available at github.com/davidcato/monteLLTB.

References

Abdalla E., et al., 2022, *Journal of High Energy Astrophysics*, 34, 49, [2203.06142].
Aghanim N., et al., 2018, [1807.06209].
Aghanim N., et al., 2020, *Astron. Astrophys.*, 641, A1, [1807.06205].
Alam S., et al., 2017, *Mon. Not. Roy. Astron. Soc.*, 470, 2617, [1607.03155].
Alnes H., Amarzguioui M., 2006, *Phys. Rev. D*, 74, 103520, [astro-ph/0607334].
Audren B., Lesgourgues J., Benabed K., Prunet S., 2013, *JCAP*, 1302, 001, [1210.7183].
Beutler F., et al., 2011, *Mon. Not. Roy. Astron. Soc.*, 416, 3017, [1106.3366].
Böhringer H., Chon G., Collins C. A., 2020, *Astron. Astrophys.*, 633, A19, [1907.12402].
Bolejko K., 2007, *Phys. Rev. D*, 75, 043508, [astro-ph/0610292].
Bose B., Lombriser L., 2021, *Phys. Rev. D*, 103, L081304, [2006.16149].
Brinckmann T., Lesgourgues J., 2018, [1804.07261].
Burnham K. P., Anderson D. R., 2002, *Model selection and multimodel inference*, 2, 70.
Cai R.-G., Ding J.-F., Guo Z.-K., Wang S.-J., Yu W.-W., 2021, *Phys. Rev. D*, 103, 123539, [2012.08292].
Camarena D., Marra V., 2018, *Phys. Rev.*, D98, 023537, [1805.09900].
Camarena D., Marra V., 2020, *Phys. Rev. Res.*, 2, 013028, [1906.11814].
Camarena D., Marra V., 2021, *Mon. Not. Roy. Astron. Soc.*, 504, 5164, [2101.08641].
Camarena D., Marra V., Sakr Z., Clarkson C., 2022, *Mon. Not. Roy. Astron. Soc.*, 509, 1291, [2107.02296].
Castello S., Högbås M., Mörtzell E., 2021, [2110.04226].
Clarkson C., Regis M., 2011, *JCAP*, 02, 013, [1007.3443].
Colgáin E. O., Sheikh-Jabbari M. M., Solomon R., Bargiacchi G., Capozziello S., Dainotti M. G., Stojkovic D., 2022, [2203.10558].
Courtois H. M., Pomaredé D., Tully R. B., Courtois D., 2013, *Astron. J.*, 146, 69, [1306.0091].
Di Valentino E., Melchiorri A., Silk J., 2019, *Nature Astron.*, 4, 196, [1911.02087].
Ding Q., Nakama T., Wang Y., 2020, *Sci. China Phys. Mech. Astron.*, 63, 290403, [1912.12600].

Efstathiou G., 2021, *Mon. Not. Roy. Astron. Soc.*, 505, 3866, [2103.08723].
Fixsen D., Cheng E., Gales J., Mather J. C., Shafer R., Wright E., 1996, *Astrophys. J.*, 473, 576, [astro-ph/9605054].
Frith W. J., Busswell G. S., Fong R., Metcalfe N., Shanks T., 2003, *Mon. Not. Roy. Astron. Soc.*, 345, 1049, [astro-ph/0302331].
Gelman A., Rubin D. B., 1992, *Statist. Sci.*, 7, 457.
Handley W., 2021, *Phys. Rev. D*, 103, L041301, [1908.09139].
Haslbauer M., Banik I., Kroupa P., 2020, *Mon. Not. Roy. Astron. Soc.*, 499, 2845, [2009.11292].
Hoscheit B. L., Barger A. J., 2018, *Astrophys. J.*, 854, 46, [1801.01890].
Ivanov M. M., Ali-Haïmoud Y., Lesgourgues J., 2020, *Phys. Rev. D*, 102, 063515, [2005.10656].
Jeffreys H., 1961, *International series of monographs on physics*.
Keenan R. C., Barger A. J., Cowie L. L., 2013, *Astrophys. J.*, 775, 62, [1304.2884].
Kenworthy W. D., Scolnic D., Riess A., 2019, *Astrophys. J.*, 875, 145, [1901.08681].
Kolb E. W., Marra V., Matarrese S., 2010, *Gen. Rel. Grav.*, 42, 1399, [0901.4566].
Lewis A., 2019, [1910.13970].
Lin W., Ishak M., 2017, *Phys. Rev. D*, 96, 023532, [1705.05303].
Luković V. V., Haridasu B. S., Vittorio N., 2020, *Mon. Not. Roy. Astron. Soc.*, 491, 2075, [1907.11219].
Marra V., Notari A., 2011, *Class.Quant.Grav.*, 28, 164004, [1102.1015].
Marra V., Amendola L., Sawicki I., Valkenburg W., 2013, *Phys. Rev. Lett.*, 110, 241305, [1303.3121].
Marra V., Castro T., Camarena D., Borgani S., Ragagnin A., 2022, [2203.04009].
Moresco M., 2015, *Mon. Not. Roy. Astron. Soc.*, 450, L16, [1503.01116].
Moresco M., et al., 2012, *JCAP*, 08, 006, [1201.3609].
Moresco M., et al., 2016, *JCAP*, 05, 014, [1601.01701].
Moresco M., et al., 2022, [2201.07241].
Odderskov I., Hannestad S., Brandbyge J., 2017, *JCAP*, 03, 022, [1701.05391].
Perivolaropoulos L., Skara F., 2021, [2105.05208].
Redlich M., Bolejko K., Meyer S., Lewis G. F., Bartelmann M., 2014, *Astron. Astrophys.*, 570, A63, [1408.1872].
Reichardt C., et al., 2020, [2002.06197].
Reid M., Pesce D., Riess A., 2019, *Astrophys. J. Lett.*, 886, L27, [1908.05625].
Riess A. G., et al., 2016, *Astrophys. J.*, 826, 56, [1604.01424].
Riess A. G., et al., 2021, [2112.04510].
Ross A. J., Samushia L., Howlett C., Percival W. J., Burden A., Manera M., 2015, *Mon. Not. Roy. Astron. Soc.*, 449, 835, [1409.3242].
Scolnic D., et al., 2018, *Astrophys. J.*, 859, 101, [1710.00845].
Simon J., Verde L., Jimenez R., 2005, *Phys. Rev. D*, 71, 123001, [astro-ph/0412269].
Stern D., Jimenez R., Verde L., Kamionkowski M., Stanford S., 2010, *JCAP*, 02, 008, [0907.3149].
Szekeres P., 1975, *Communications in Mathematical Physics*, 41, 55.
Tokutake M., Ichiki K., Yoo C.-M., 2018, *JCAP*, 03, 033, [1712.04229].
Trotta R., 2008, *Contemp. Phys.*, 49, 71, [0803.4089].
Vagnozzi S., Di Valentino E., Gariazzo S., Melchiorri A., Mena O., Silk J., 2021a, *Phys. Dark Univ.*, 33, 100851, [2010.02230].
Vagnozzi S., Loeb A., Moresco M., 2021b, *Astrophys. J.*, 908, 84, [2011.11645].
Valkenburg W., 2012, *Gen. Rel. Grav.*, 44, 2449, [1104.1082].
Valkenburg W., Marra V., Clarkson C., 2014, *Mon. Not. Roy. Astron. Soc.*, 438, L6, [1209.4078].
Whitbourn J. R., Shanks T., 2014, *Mon. Not. Roy. Astron. Soc.*, 437, 2146, [1307.4405].

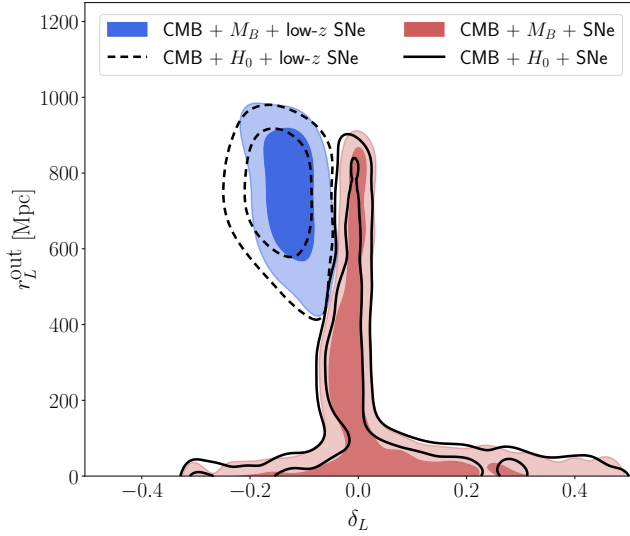


Figure A1. Marginalized constraints on the effective mass density contrast δ_L and compensating scale r_L^{out} of the Λ LTB model in a flat background Universe at 68% and 95% confidence level.

$\ln B_{01}$	Strength of evidence
> 5	Strong evidence for Λ CDM
$[2.5, 5]$	Moderate evidence for Λ CDM
$[1, 2.5]$	Weak evidence for Λ CDM
$[-1, 1]$	Inconclusive
$[-2.5, -1]$	Weak evidence for Λ LTB
$[-5, -2.5]$	Moderate evidence for Λ LTB
< -5	Strong evidence for Λ LTB

Table B1. Conservative Jeffreys' scale (Trotta 2008).

Wong J. H. W., Shanks T., Metcalfe N., Whitbourn J. R., 2021, [\[10.1093/mnras/stac396, \[2107.08505\]\]](#).
 Zhang C., Zhang H., Yuan S., Zhang T.-J., Sun Y.-C., 2014, *Res. Astron. Astrophys.*, 14, 1221, [\[1207.4541\]](#).
 Zibin J. P., 2008, *Phys. Rev. D*, 78, 043504, [\[0804.1787\]](#).

APPENDIX A: RESULTS WITH THE PRIOR ON H_0

Here, for completeness, we compare the constraints that are obtained using the prior on M_B with the ones obtained using the prior on local H_0 , see Figure A1. We can see that the two choices provide very similar constraints thanks to the way we implemented the prediction of the local Hubble rate, see Section 2.3.

APPENDIX B: QUALITATIVE INTERPRETATION OF BAYES RATIO AND Δ AIC

Tables B1 and B2 present the scales that we adopt for the interpretation of the quantitative results from model selection via the Bayes ratio and Δ AIC.

$ \Delta\text{AIC} $	Level of empirical support for the model with the higher AIC
0 – 2	Substantial
4 – 7	Considerably less
> 10	Essentially none

Table B2. Qualitative interpretation of Δ AIC according to the calibrated Jeffreys' scale (Burnham & Anderson 2002).